Metrol. Meas. Syst., Vol. 31 (2024) No. 2, pp. 383–399
DOI: 10.24425/mms.2024.149705

PAN POLSKA AKADEMIA NAUK

METROLOGY AND MEASUREMENT SYSTEMS

Index 330930, ISSN 0860-8229
www.metrology.wat.edu.pl

M&MS

AN ADAPTIVE ESTIMATION OF GROUND VEHICLE STATE WITH UNKNOWN MEASUREMENT NOISE

Yan Wang[1)], Xuan Sun[2)], Dong Cui[3)], Xianfang Wang[4)], Zhijuan Jia[5)], Zhiguo Zhang[6)]

1) The Hong Kong Polytechnic University, Department of Industrial and Systems Engineering, Hong Kong, China
2) The Beijing Jiaotong University, School of Traffic and Transportation, Beijing, China
3) CATARC (Tianjin) Automotive Engineering Research Institute Co., Ltd., Tianjin 300300, China
4) School of Computer Science & Technology, Henan Institute of Technology, Xinxiang 453003, China
5) School of Information Science and Technology, Zhengzhou Normal University, Zhengzhou 450044, Henan, China
6) School of Mechanical Engineering, Southeast University, Nanjing 211189, China,(✉ *230198933@seu.edu.cn*)

Abstract

Accurate information about the vehicle state such as sideslip angle is critical for both advanced assisted driving systems and driverless driving. These vehicle states are used for active safety control and motion planning of the vehicle. Since these state parameters cannot be directly measured by onboard sensors, this paper proposes an adaptive estimation scheme in case of unknown measurement noise. Firstly, an estimation method based on the bicycle model is established using a square-root cubature Kalman filter (SQCKF), and secondly, the expectation maximization (EM) approach is used to dynamically update the statistic parameters of measurement noise and integrate it into SQCKF to form a new expectation maximization square-root cubature Kalman filter (EMSQCKF) algorithm. Simulations and experiments show that EMSQCKF has higher estimation accuracy under different driving conditions compared to the unscented Kalman filter.

Keywords: vehicle state estimation, square-root cubature Kalman filter, measurement noise, expectation-maximization method.

1. Introduction

With the advancement of intelligent vehicle technology, the significance of advanced driver assistance systems, such as electronic stability control systems and collision avoidance systems, among active safety systems is progressively escalating. Ensuring optimal performance of these life-saving systems necessitates a precise comprehension of the vehicle motion state [1]. Unfortunately, some states such as sideslip angle and longitudinal velocity cannot be directly measured using in-vehicle sensors [2]. Consequently, there is a pressing need for reliable online estimation algorithms.

Kinematics-based approaches, commonly employing diverse sensor measurements, have found extensive application in vehicle state estimation. One such approach is the utilization of data

Article history: received December 23, 2023; revised February 21, 2024; accepted March 17, 2024; available online April 8, 2024.

from the *Global Positioning System* (GPS) to estimate the states like the sideslip angle and tire cornering stiffness [3]. Similar studies such as [4, 5] have also demonstrated that this type of method has higher estimation accuracy when the vehicle is in linear operating conditions. Even though kinematics-based methods are easy to be implemented, they are vulnerable to sensor error, potential sensor failures, and the risk of GPS malfunctions. Furthermore, their effectiveness is hampered by either low update frequency or high cost associated with GPS equipment [6]. In response to the challenges posed by kinematics-based estimation methods, numerous experts have advocated for dynamic-based state estimation approaches. These methods typically necessitate information on vehicle inertial parameters and tire model parameters. Methods that utilize these dynamics models in combination with advanced filtering are receiving increasing attention. For example, the Kalman filter was utilized to predict the roll angle and sideslip angle [7]. Due to the fact that the traditional Kalman filter is primarily designed for linear problems, whereas the *Extended Kalman Filter* (EKF) excels in addressing nonlinear filtering challenges, and considering the inherent complexity of a vehicle as a nonlinear system, methodologies based on EKF have been extensively employed for vehicle state estimation. Exemplary instances include the application of EKF for the estimation of sideslip angle [8] and tire forces [9], as well as the estimation of other vehicle states leveraging tire force information [10]. To enhance the adaptability of the EKF, some improved variants, such as the variable structure EKF [11] and interactive multiple model EKF [12], have proven to be effective estimation methods. Concurrently, the H-infinity EKF designed to accommodate noise uncertainties [13] has also been developed for the estimation of vehicle speed and mass parameters.

Due to its superior performance in handling nonlinear filtering challenges, the *Unscented Kalman Filter* (UKF) often outperforms the EKF in terms of estimation accuracy of vehicle state. Examples include the double UKF [14] and the adaptive UKF [15, 16]. Additionally, estimating longitudinal velocity while considering the impact of tire deformation is an effective method to enhance estimation accuracy [17]. To further enhance the estimation accuracy, a hybrid UKF [18] and a variable structure UKF [19] as well as a weight fusion UKF [20] have been proposed. To enhance the adaptive nature of the algorithm, the interactive multi-model UKF is also a worthwhile research direction [21]. The UKF is proficient at enhancing the estimation performance of nonlinear systems; however, when dealing with certain high-dimensional nonlinear dynamical systems, stability may be a concern. The *Cubature Kalman Filter* (CKF) adopts a numerical integration approach for Gaussian filters and it surpasses the UKF in numerical stability and estimation performance. Therefore, CKF is promising for vehicle state estimation [22]. Addressing the challenge posed by unknown noise, robust CKFs have been introduced to improve estimation performance [23–25]. Furthermore, higher-order CKFs have been employed to predict vehicle states [26]. The estimation performance can also be effectively improved by dynamically updating the measurement noise matrix of the CKF using fuzzy logic systems [27]. Some researchers have taken a model adaptation approach to enhance the estimation accuracy. The interactive multi-model CKF [28] fuses the results from different models to enhance overall accuracy. Furthermore, the *square-root CKF* (SQCKF) exhibits several advantages over the traditional CKF. Firstly, it enhances numerical stability by representing the covariance matrix in the *square root* (SR) form. Unlike CKF, SQCKF avoids the Cholesky decomposition. Additionally, SQCKF tends to be more computationally efficient, especially in large-scale systems or high-dimensional state spaces. Considering the performance advantages of SQCKF, this paper utilizes SQCKF for vehicle state estimation. In addition, considering the uncertainty of measurement noise, a noise covariance online updating algorithm based on *expectation maximization* (EM) is designed, which is embedded in the SQCKF to form the EMSQCKF for estimating vehicle state. The special contributions of this paper are listed below:

1. A SQCKF-based estimator based on in-vehicle sensors is designed to simultaneously predict sideslip angle, yaw rate, and vehicle speed. The estimation performance of the proposed method outperforms the conventional UKF and also saves estimation costs by avoiding the utilization of additional sensors.
2. Considering the effect of measurement noise, an EM algorithm is used to optimize the performance of the SQCKF, and by combining the two to form a new EMSQCKF, it is possible to achieve more accurate estimation with unknown noise.
3. Simulations and experiments show that EMSQCKF has the highest estimation accuracy under different driving conditions compared to UKF and SQCKF and further show that the proposed algorithm is insensitive to the changes in driving conditions and has a strong adaptive capability.

The rest of this paper is organized as follows. The vehicle model and problem formation are depicted in Section 2. The EMSQCKF is presented in Section 3. Experimental results and discussion are shown in Section 4. Section 5 concludes the work.

2. Vehicle model and problem formation

We opt for the bicycle model as delineated in reference [25] to characterize the dynamic response of the vehicle. The impact of air resistance and the suspension system is disregarded. The front wheels share identical steering angles, while the rear wheels do not have steering capabilities. Additionally, the centre of vehicle gravity is presumed to coincide with the origin of the coordinate system. For a more detailed derivation of the bicycle model see [29]. Fig. 1 shows a schematic representation of this model. The expressions are provided in the following equations.

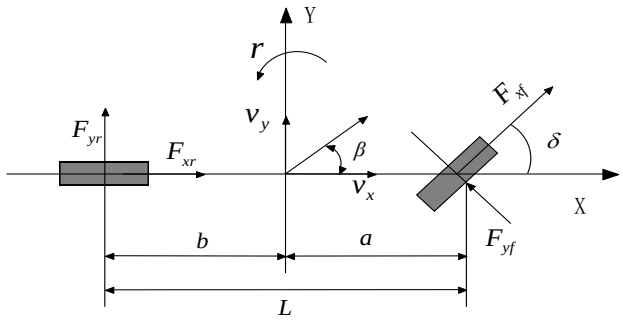

Fig. 1. Bicycle model.

$$\dot{r} = \frac{a^2 k_1 + b^2 k_2}{I_z v_x} r + \frac{a k_1 - b k_2}{I_z} \beta - \frac{a k_1}{I_z} \delta, \tag{1}$$

$$\dot{\beta} = \left(\frac{a k_1 - b k_2}{m v_x^2} - 1 \right) r + \frac{k_1 + k_2}{m v_x} \beta - \frac{k_1}{m v_x} \delta, \tag{2}$$

$$\dot{v}_x = r \beta v_x + a_x, \tag{3}$$

$$a_y = \frac{a k_1 - b k_2}{m v_x} r + \frac{k_1 + k_2}{m} \beta - \frac{k_1}{m} \delta, \tag{4}$$

where β is sideslip angle, v_x represents longitudinal vehicle velocity, v_y represents lateral vehicle velocity, k_1 and k_2 are the front and rear tire cornering stiffnesses, L is the wheelbase, m is vehicle

mass, a and b are distances from the center of gravity to front axle and rear axle, a_x and a_y are longitudinal and lateral acceleration, δ is front wheel steering angle, r is yaw rate. F_x and F_y represent the longitudinal and lateral tire forces, respectively.

Based upon the formulations above, the discrete vehicle state-space model is articulated as follows

$$\begin{cases} x_k = f(x_{k-1}, u_{k-1}) + W_{k-1} \\ z_k = h(x_k, u_k) + V_k \end{cases} \tag{5}$$

$$x_k = [r, \beta, v_x]^T, \quad z_k = [a_y]^T, \quad u_k = [\delta, a_x]^T.$$

The discrete vehicle state-space model is given by:

$$\begin{bmatrix} r_k \\ \beta_k \\ v_{x,k} \end{bmatrix} = \begin{bmatrix} r_{k-1} + \left(\dfrac{a^2 k_1 + b^2 k_2}{I_z v_{x,k-1}} r_{k-1} + \dfrac{a k_1 - b k_2}{I_z} \beta_{k-1} - \dfrac{a k_1}{I_z} \delta \right) \Delta t \\ \beta_{k-1} + \left[\left(\dfrac{a k_1 - b k_2}{m v_{x,k-1}^2} - 1 \right) r_{k-1} + \dfrac{k_1 + k_2}{m v_{x,k-1}} \beta_{k-1} - \dfrac{k_1}{m v_{x,k-1}} \delta \right] \Delta t \\ v_{x,k-1} + \left(r_{k-1} \beta_{k-1} v_{x,k-1} + a_x \right) \Delta t \end{bmatrix}, \tag{6}$$

where h is the measurement output function, Δt is the sampling interval, W_k represents the process noise with a covariance matrix Q_k, V_k denotes the measurement noise with a covariance matrix R_k, f is the state transition function, x_k is the state vector, k signifies the sampling instant, the measurement vector is denoted as z_k, the input vector is u_k.

3. Methodology

In this section, the comprehensive estimation flowchart utilizing EMSQCKF is pictured in Fig. 2. Initially, sensor signals from the actual vehicle are simultaneously input into both EM algorithm module and time update steps of SQCKF. Specifically, the input signal in the EM is the lateral acceleration, while the SQCKF input signal mainly includes the front wheel angle and longitudinal acceleration. The EM algorithm dynamically adjusts the measurement noise based on the vehicle model, a priori statistic parameters of measurement noise, and the lateral acceleration signal. Subsequently, the updated noise is integrated into the measurement update process of SQCKF, creating EMSQCKF, which facilitates the simultaneous estimation of sideslip angle, yaw rate, and vehicle velocity. The iterative intricacies of the internal EMSQCKF process are detailed in Table 1.

3.1. SQCKF

The SQCKF [30] stands out as an optimal state estimator, harnessing the power of a deterministic sampling mechanism. It not only involves the transmission of the SR of the prediction error covariance but also integrates the crucial element of the posterior error covariance. This ensures that the covariance matrix maintains both symmetry and positive definiteness [31].

The SQCKF unfolds through the following iterative steps:

1. Initialization:

$$\hat{x}_0 = E(x_0), \tag{7}$$

$$S_0 = E[(x_0 - \hat{x}_0)(x_0 - \hat{x}_0)^T], \tag{8}$$

where E is mathematical expectation, S is the covariance matrix.

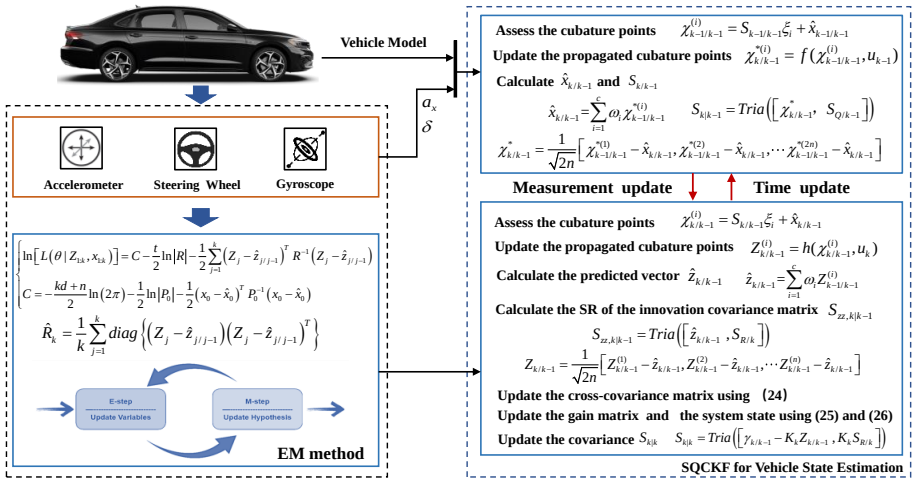

Fig. 2. Scheme of the EMSQCKF.

Calculate cubature points ξ_i and weights ω_i can be defined as follows:

$$\omega_i = \frac{1}{c},\ \xi_i = \sqrt{\frac{c}{2}}\left[\begin{pmatrix}1\\0\\\vdots\\0\end{pmatrix}\cdots\begin{pmatrix}0\\0\\\vdots\\1\end{pmatrix}\begin{pmatrix}-1\\0\\\vdots\\0\end{pmatrix}\cdots\begin{pmatrix}0\\0\\\vdots\\-1\end{pmatrix}\right],\quad i=1,2,\cdots c,\ c=2n, \tag{9}$$

where variable c represents the quantity of cubature points, and n is the dimension of x_k.

$$\prod_{k-1/k-1} = S_{k-1/k-1}S_{k-1/k-1}^T, \tag{10}$$

$$Q_{k-1} = S_{Q/k-1}S_{Q/k-1}^T, \tag{11}$$

$$R_k = S_{R/k}S_{R/k}^T, \tag{12}$$

$S_{k-1/k-1}$ is a SR of the covariance matrix, $\prod_{k-1/k-1}$, $S_{Q/k-1}$ is a SR of the Q_{k-1}, and $S_{R/k}$ is a SR of the R_k.

2. Time update:
Assess the cubature points

$$\chi_{k-1/k-1}^{(i)} = S_{k-1/k-1}\xi_i + \hat{x}_{k-1/k-1}. \tag{13}$$

Update the propagated cubature points

$$\chi_{k/k-1}^{*(i)} = f(\chi_{k-1/k-1}^{(i)}u_{k-1}). \tag{14}$$

Calculate $\hat{x}_{k/k-1}$ and $S_{k/k-1}$

$$\hat{x}_{k/k-1} = \sum_{i=1}^{c}\omega_i\chi_{k-1/k-1}^{*(i)}, \tag{15}$$

$$S_{k|k-1} = Tria\left(\left[\chi_{k/k-1}^{*}, S_{Q/k-1}\right]\right). \tag{16}$$

Tria() is the QR decomposition of the matrix.

$$\chi^{*}_{k/k-1} = \frac{1}{\sqrt{2n}}\left[\chi^{*(1)}_{k-1/k-1} - \hat{x}_{k/k-1}, \chi^{*(2)}_{k-1/k-1} - \hat{x}_{k/k-1}, \cdots \chi^{*(2n)}_{k-1/k-1} - \hat{x}_{k/k-1}\right]. \quad (17)$$

3. Measurement update:
Assess the cubature points

$$\chi^{(i)}_{k/k-1} = S_{k/k-1}\xi_i + \hat{x}_{k/k-1}. \quad (18)$$

Calculate the propagated cubature points

$$Z^{(i)}_{k/k-1} = h(\chi^{(i)}_{k/k-1}u_k). \quad (19)$$

Calculate the predicted vector $\hat{z}_{k/k-1}$

$$\hat{z}_{k/k-1} = \sum_{i=1}^{c} \omega_i Z^{(i)}_{k-1/k-1}. \quad (20)$$

Calculate the SR of the innovation covariance matrix $S_{zz,k|k-1}$

$$S_{zz,k|k-1} = Tria\left(\left[\hat{z}_{k/k-1}, S_{R/k}\right]\right), \quad (21)$$

$$Z_{k/k-1} = \frac{1}{\sqrt{2n}}\left[Z^{(1)}_{k/k-1} - \hat{z}_{k/k-1}, Z^{(2)}_{k/k-1} - \hat{z}_{k/k-1}, \cdots Z^{(n)}_{k/k-1} - \hat{z}_{k/k-1}\right]. \quad (22)$$

Update the cross-covariance matrix $S_{xz,k|k-1}$

$$\gamma_{k/k-1} = \frac{1}{\sqrt{2n}}\left[\chi^{(1)}_{k/k-1} - \hat{x}_{k/k-1}, \chi^{(2)}_{k/k-1} - \hat{x}_{k/k-1}, \cdots \chi^{(2}_{k/k-1}n) - \hat{x}_{k/k-1}\right], \quad (23)$$

$$S_{xz,k|k-1} = \gamma_{k/k-1}Z^{T}_{k/k-1}. \quad (24)$$

Update the gain matrix K_k, the system state $\hat{x}_{k/k}$, and the covariance $S_{k|k}$

$$K_k = \left(\left(S_{xz,k|k-1}/S_{zz,k|k-1}\right)/S_{zz,k|k-1}\right), \quad (25)$$

$$\hat{x}_{k/k} = \hat{x}_{k/k-1} + K_k(z_k - Z_{k/k-1}), \quad (26)$$

$$S_{k|k} = Tria\left(\left[\gamma_{k/k-1} - K_k Z_{k/k-1}, K_k S_{R/k}\right]\right). \quad (27)$$

3.2. Updating noise using the expectation maximization method

Due to factors such as sensor aging, the measurement data includes uncertain measurement noise. Additionally, the diversity of vehicle types and sensors leads to varied statistical characteristics of measurement noise. We posit that the unidentified noise parameters are represented by $\theta = R$. Employing the Maximum Likelihood criterion, we can subsequently initiate the estimation procedure.

$$\theta^{\mathrm{ML}} = \arg\max L\theta|Z_{1:k}, \quad (28)$$

where θ^{ML} is the Maximum Likelihood estimation of θ.

Next, we will leverage the Maximum Expectation algorithm framework to obtain a measurement noise adaptive update algorithm. We will then integrate this algorithm into the SQCKF, forming an EMSQCKF. The EM method comprises two iterative stages: the *Expectation step* (E-step) and the *Maximization step* (M-step). During the E-step, the algorithm calculates the anticipated value of the likelihood function. In the M-step, the algorithm determines the values of the noise parameters that maximize the likelihood function and utilizes them to update the measurement noise variance.

1. E-step
Drawing upon the Markov properties as well as the definitions of the likelihood function and conditional probability, we can decompose the likelihood function with respect to θ in the following manner:

$$L\left(\theta|Z_{1:k}, x_{1:k}\right) = p\left(Z_{1:k}, x_{1:k}|\theta\right) = p\left(X_0|\theta\right)\prod_{j=1}^{k} p\left(x_j|x_{j-1}, \theta\right)\prod_{j=1}^{k} p\left(Z_j|x_j, \theta\right), \tag{29}$$

where $Z_{1:k} = \left(Z_j\right)_{j=1}^{k}$, $x_{1:k} = \left(x_j\right)_{j=1}^{k}$ and $p(\cdot)$ is the probability density function.
The formulation for the conditional probability of the initial state vector $x_0 \sim N(x_0, P_0)$ is as follows:

$$p\left(x_0|\theta\right) = (2\pi)^{-\frac{n}{2}}\left|P_0\right|^{-\frac{1}{2}}\exp\left\{-\frac{1}{2}\left(x_0 - \hat{x}_0\right)^T P_0^{-1}\left(x_0 - \hat{x}_0\right)\right\}, \tag{30}$$

where $N(\mu, \Sigma)$ denotes the Gaussian distribution with mean μ and variance Σ, n signifies the dimension of state observation, and $|\cdot|$ denotes the determinant of the covariance matrix.
Based on (20), we can derive the following expression:

$$p\left(Z_j|x_j, \theta\right) = (2\pi)^{-\frac{d}{2}}\left|R\right|^{-\frac{1}{2}}\exp\left\{-\frac{1}{2}\left(Z_j - \hat{z}_{j/j-1}\right)^T R^{-1}\left(Z_j - \hat{z}_{j/j-1}\right)\right\}, \tag{31}$$

where d is the dimension of data.
Based on (29)–(31), the corresponding log-likelihood function for (31) is as follows:

$$\begin{cases} \ln\left[L\left(\theta|Z_{1:k}, x_{1:k}\right)\right] = C - \dfrac{t}{2}\ln|R| - \dfrac{1}{2}\displaystyle\sum_{j=1}^{k}\left(Z_j - \hat{z}_{j/j-1}\right)^T R^{-1}\left(Z_j - \hat{z}_{\frac{j}{j-1}}\right) \\ C = -\dfrac{kd+n}{2}\ln(2\pi) - \dfrac{1}{2}\ln|P_0| - \dfrac{1}{2}\left(x_0 - \hat{x}_0\right)^T P_0^{-1}\left(x_0 - \hat{x}_0\right) \end{cases}, \tag{32}$$

where x_0 and P_0 are solely dependent on the initial state, it follows that C remains constant.
By computing the mathematical expectation of (32), we obtain:

$$J = E\left\{\ln\left[L\left(\theta|Z_{1:k}, x_{1:k}\right)\right]\right\} = C - \frac{\tau}{2}\ln|R| - \frac{1}{2}\sum_{j=1}^{k} E\left\{\left(Z_j - \hat{z}_{j/j-1}\right)^T R^{-1}\left(Z_j - \hat{z}_{j/j-1}\right)\right\} \tag{33}$$

2. M-step
The process of estimating parameters that maximize the function (33) is accomplished through the utilization of the gradient descent algorithm.

$$\frac{\partial J}{\partial R} = 0. \tag{34}$$

Moreover, taking into account that the noise matrix is diagonal, we have

$$\hat{R}_k = \frac{1}{k}\sum_{j=1}^{k}\operatorname{diag}\left\{\left(Z_j - \hat{z}_{j/j-1}\right)\left(Z_j - \hat{z}_{j/j-1}\right)^T\right\}. \tag{35}$$

To further facilitate real-time computation, we write it down in the recursive form

$$\begin{aligned}\hat{R}_k &= \frac{1}{k}\sum_{j=1}^{k-1}\operatorname{diag}\left[\left(Z_j-\hat{z}_{j/j-1}\right)\left(Z_j-\hat{z}_{j/j-1}\right)^T\right]\\ &\quad+\frac{1}{k}\operatorname{diag}\left[\left(Z_j-\hat{z}_{j/j-1}\right)\left(Z_j-\hat{z}_{j/j-1}\right)^T\right]\\ &= \frac{1}{k}\left\{(k-1)\hat{R}_{k-1}+\operatorname{diag}\left[\left(Z_j-\hat{z}_{j/j-1}\right)\left(Z_j-\hat{z}_{j/j-1}\right)^T\right]\right\}. \end{aligned} \tag{36}$$

Let (36) be embedded in the SQCKF forms EMSQCKF, which is iterated as follows in Table 1.

Table 1. EMSQCKF method.

Estimation Framework
Step 1: Set $\hat{x}_0 = E(x_0)$, $\Pi_0 = E[(x_0-\hat{x}_0)(x_0-\hat{x}_0)^T]$ Assess cubature points ξ_i and weights ω_i $\omega_i = \frac{1}{c}, \quad \xi_i = \sqrt{\frac{c}{2}}\left[\begin{pmatrix}1\\0\\\vdots\\0\end{pmatrix}\cdots\begin{pmatrix}0\\0\\\vdots\\1\end{pmatrix}\begin{pmatrix}-1\\0\\\vdots\\0\end{pmatrix}\cdots\begin{pmatrix}0\\0\\\vdots\\-1\end{pmatrix}\right], \quad i=1,2,\cdots c, c=2n$
Step 2: Time update Assess the cubature points: $\chi^{(i)}_{k-1/k-1} = S_{k-1/k-1}\xi_i + \hat{x}_{k-1/k-1}$ Update the propagated cubature points: $\chi^{*(i)}_{k/k-1} = f(\chi^{(i)}_{k-1/k-1}u_{k-1})$ Update the predicted state $\hat{x}_{k/k-1}$ and $S_{k/k-1}$: $\hat{x}_{k/k-1} = \sum_{i=1}^{c}\omega_i\chi^{*(i)}_{k-1/k-1}, S_{k\|k-1} = Tria\left(\left[\chi^*_{k/k-1}, S_{Q/k-1}\right]\right)$ $\chi^*_{k/k-1} = \frac{1}{\sqrt{2n}}\left[\chi^{*(1)}_{k-1/k-1}-\hat{x}_{k/k-1}, \chi^{*(2)}_{k-1/k-1}-\hat{x}_{k/k-1}, \cdots \chi^{*(2n)}_{k-1/k-1}-\hat{x}_{k/k-1}\right]$
Step 3: Measurement update Assess the cubature points: $\chi^{(i)}_{k/k-1} = S_{k/k-1}\xi_i + \hat{x}_{k/k-1}$ Calculate the propagated cubature points: $Z^{(i)}_{k/k-1} = h(\chi^{(i)}_{k/k-1}u_k)$ Calculate the predicted measurement vector: $\hat{z}_{k/k-1} = \sum_{i=1}^{c}\omega_i Z^{(i)}_{k-1/k-1}$ Calculate the square-root of the innovation covariance matrix $S_{zz,k\|k-1}$ $\hat{R}_k = \frac{1}{k}\left\{(k-1)\hat{R}_{k-1}+\operatorname{diag}\left[\left(Z_j-\hat{z}_{j/j-1}\right)\left(Z_j-\hat{z}_{j/j-1}\right)^T\right]\right\},$ $\hat{R}_k = S_{R/k}S^T_{R/k}$, $S_{zz,k\|k-1} = Tria\left(\left[\hat{z}_{k/k-1}, S_{R/k}\right]\right)$ Calculate the cross-covariance matrix $S_{xz,k\|k-1}$ using (21) The filter gain K_k and $\hat{x}_{k/k}$ are calculated with (25) and (22). Update the covariance $S_{k\|k} = Tria\left(\left[\gamma_{k/k-1}-K_kZ_{k/k-1}, K_kS_{R/k}\right]\right)$
Step 4: At the next iteration loop, Steps 2 to 3 will be repeated.

Metrol. Meas. Syst., Vol. 31 (2024), No. 2, pp. 383–399
DOI: 10.24425/mms.2024.149705

4. Results and discussion

4.1. Simulation test

Simulation experiments are performed to validate the EMSQCKF. During the testing phase, the output values from the Carsim software are compared with the estimated values derived from SQCKF and UKF. In the simulation environment, the vehicle driving on a wet asphalt road (see Fig. 3), performed a lane change at a velocity of 54 km/h. Figs. 4 and 5 illustrate the front wheel angle and the lateral acceleration.

Fig. 3. Double lane change test on a wet asphalt road.

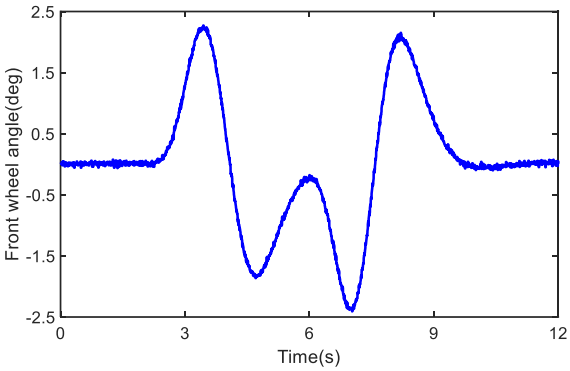

Fig. 4. Front wheel angle on a wet asphalt road.

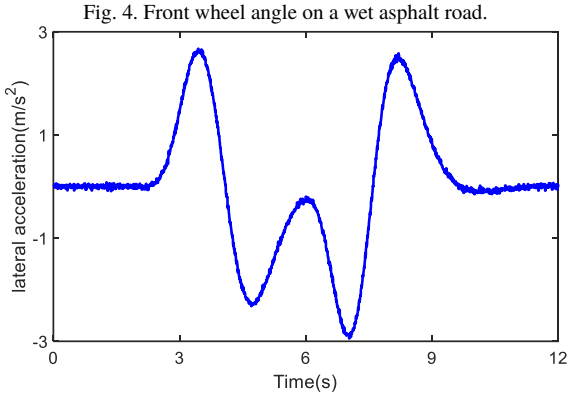

Fig. 5. Lateral acceleration on a wet asphalt road.

In Figure 6, the yaw rate estimation outcomes obtained through various approaches are displayed. The red solid line represents the vehicle state output from the Carsim software, serving as a reference value. Due to the dynamic nature of driving conditions and the ever-changing operational environment of the sensors, the measurement noise parameters undergo continuous variations. To compare the impact of dynamic noise updates, the noise parameters of the three estimation algorithms are artificially set to deviate from their true values. Observably, SQCKF exhibits superior performance over UKF, attributed to CKF's numerical stability advantages and its utilization of cubature points. Furthermore, EMSQCKF surpasses both SQCKF and UKF in terms of estimation accuracy. Within EMSQCKF, the noise parameters undergo dynamic adjustments via the EM method, allowing EMSQCKF to adapt to diverse operational conditions.

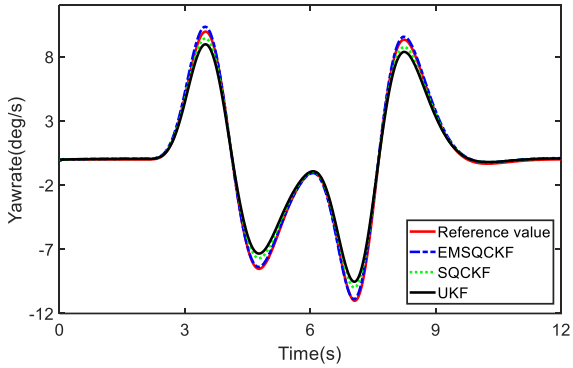

Fig. 6. Yaw rate on a wet asphalt road.

Table 2. RMSE of different methods on a wet asphalt road.

Symbol	β	v_x	r
UKF	0.0197	0.1255	0.1811
SQCKF	0.0169	0.0128	0.1194
EMSQCKF	**0.0142**	**0.0092**	**0.0519**

In Figs. 7 and 8, the estimation outcomes for vehicle velocity and sideslip angle are depicted, respectively. Notably, among the three methods, EMSQCKF consistently yields the most accurate estimation results. To provide a clearer representation of estimation errors, we employ the *root mean square error* (RMSE) as a metric for assessing the estimation accuracy of different algorithms. As presented in Table 2, EMSQCKF exhibits the smallest RMSE, signifying its superior estimation accuracy. Furthermore, to verify the effectiveness of our algorithm on different road surfaces, we also conducted tests on ice and snow roads, and the estimation results of different methods are shown in Table 3. It can be seen that EMSQCKF also has the best estimation performance.

Table 3. RMSE of different methods on a snow-covered road.

Symbol	β	v_x	r
UKF	0.0372	0.1758	0.2655
SQCKF	0.0358	0.0214	0.1967
EMSQCKF	**0.0331**	**0.0193**	**0.1274**

Metrol. Meas. Syst., Vol. 31 (2024), No. 2, pp. 383–399
DOI: 10.24425/mms.2024.149705

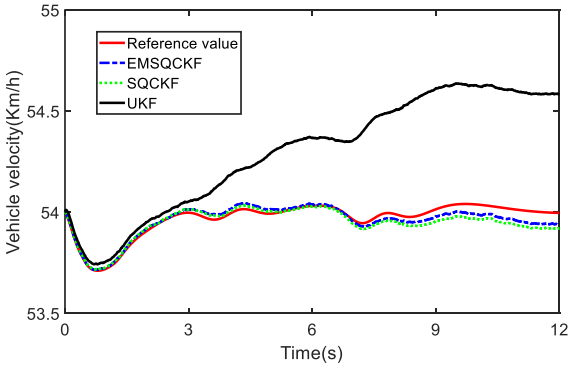

Fig. 7. Vehicle velocity on a wet asphalt road.

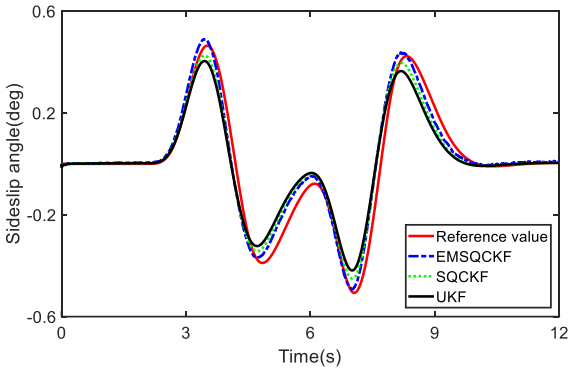

Fig. 8. Sideslip angle on a wet asphalt road.

4.2. Real vehicle test

To test the EMSQCKF approach, we initially gathered offline data from actual vehicle tests carried out on dry asphalt roads. The test scenario is illustrated in Fig. 9. For safety considerations, a steering robot is employed to execute steering manoeuvres during the real vehicle tests. The use of a steering robot offers the advantage of executing continuous steering manoeuvres with minimal fluctuation. Reference values, acquired from differential GPS measurements, are utilized for comparison with estimates generated by various algorithms.

Fig. 9. Test vehicle on a dry asphalt road.

The initial velocity is 73.7 km/h. Figs. 10 and 11 illustrate the front wheel angle and the lateral acceleration. Fig. 11 depicts the yaw rate estimation outcomes from various methods. The yaw rate estimation curve of the UKF deviates significantly from the reference value. The SQCKF surpasses the UKF in terms of estimation accuracy, which is attributed to its enhanced numerical stability and superior sampling. In the conducted test, an initial random value is assigned as the measurement noise, followed by dynamic adjustments of the noise parameters using the EM method. The results demonstrate that the EMSQCKF outperforms the standard SQCKF.

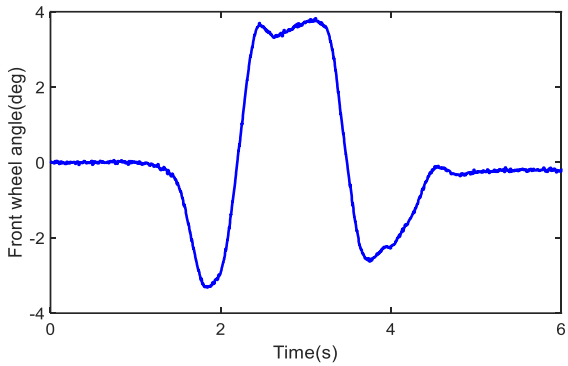

Fig. 10. Front wheel angle in the real vehicle test.

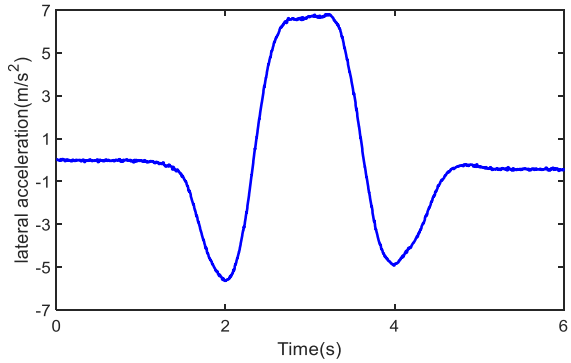

Fig. 11. Lateral acceleration in the real vehicle test.

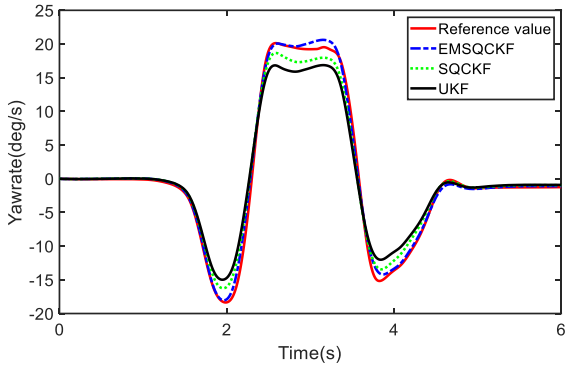

Fig. 12. Yaw rate in the real vehicle test.

Figures 13 and 14 present the outcomes of different methods for predicting vehicle speed and sideslip angle. In line with the yaw rate estimation findings, the EMSQCKF consistently provides the most accurate estimates compared to the other two methods. The results in Table 4 underscore the highest performance of the EMSQCKF, showcasing significantly lower RMSE values. This underscores the efficacy of EMSQCKF in precisely estimating the vehicle states. Moreover, the proposed algorithm exhibits optimal estimation performance in both simulation and real vehicle experiments, underscoring its strong adaptability to variations in driving conditions.

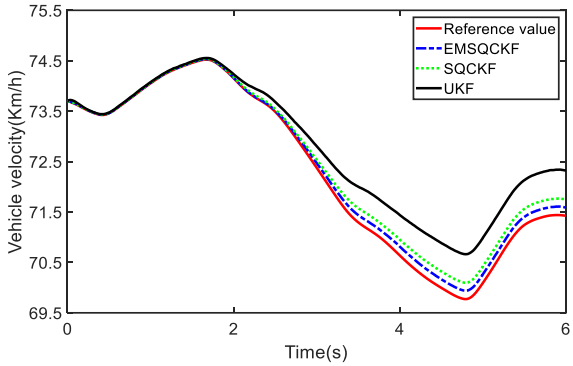

Fig. 13. Vehicle velocity in the real vehicle test.

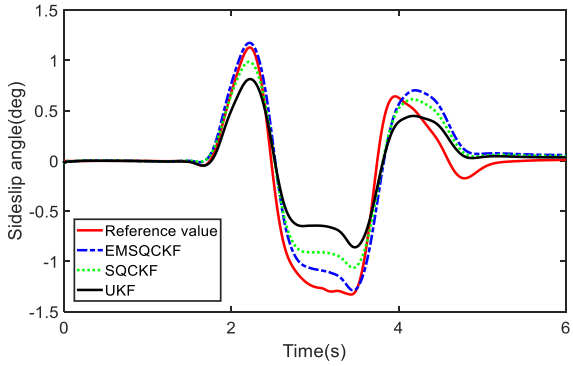

Fig. 14. Sideslip angle in the real vehicle test.

Table 4. RMSE of different methods in the real vehicle test

Symbol	β	v_x	r
UKF	0.0801	0.1861	0.6460
SQCKF	0.0551	0.0693	0.4288
EMSQCKF	**0.0530**	**0.0364**	**0.2100**

5. Conclusions

In this article, an EMSQCKF is proposed to estimate sideslip angle, yaw rate, and vehicle speed in the presence of unknown measurement noise. Utilizing the EM method, the noise parameters are dynamically updated, enabling the EMSQCKF to more accurately estimate the vehicle state

amidst unknown noise. Test results demonstrate that the EMSQCKF exhibits superior estimation accuracy compared to SQCKF and UKF in different driving conditions. This proposed method effectively provides more precise control parameters to the assisted driving system in real driving scenarios, contributing to enhanced vehicle driving safety.

Moreover, it is assumed in this study that vehicle model parameters are known in advance. In practical situations, varying usage scenarios may lead to changes in inertial parameters, such as vehicle mass, and online estimation of these parameters can further enhance the estimation accuracy. As the model-based estimation is somewhat simplified, model accuracy may be compromised under complex operating conditions. Therefore, exploring data-driven approaches for constructing vehicle models represents a valuable avenue for future research.

Acknowledgements

This work was supported by the Smart Traffic Fund (grants no. PSRI/47/2209/PR, PSRI/53/2210/PR) and supported by the National Natural Science Foundation of China (grant no. 62072157).

References

[1] Wang, Y., Hu, J., Wang, F. A., Dong, H., Yan, Y., Ren, Y., & Yin, G. (2022). Tire road friction coefficient estimation: review and research perspectives. *Chinese Journal of Mechanical Engineering*, *335*(6). https://doi.org/10.1186/s10033-021-00675-z

[2] Wang, Y., Chen, H., Yin, G., Mo, Y., de Boer, N., & Lv., C. (2024). Motion State Estimation of Preceding Vehicles with Packet Loss and Unknown Model Parameters. *IEEE/ASME Transactions on Mechatronics*. https://doi.org/10.1109/TMECH.2023.3345956

[3] Bevly, D. M., Ryu, J., & Gerdes, J. C. (2006). Integrating INS sensors with GPS measurements for continuous estimation of vehicle sideslip, roll, and tire cornering stiffness. *IEEE Transactions on Intelligent Transportation Systems*, *7*(4), 483–493. https://doi.org/10.1109/TITS.2006.883110

[4] Bevly, D. M., Gerdes, J. C., & Wilson, C. (2002). The use of GPS -based velocity measurements for measurement of sideslip and wheel slip. *Vehicle System Dynamics*, *38*(2), 127–147. https://doi.org/10.1076/vesd.38.2.127.5619

[5] Selmanaj, D., Corno, M., Panzani, G., & Savaresi, S. M. (2017). Vehicle sideslip estimation: A kinematic based approach. *Control Engineering Practice*, *67*, 1–12. https://doi.org/10.1016/j.conengprac.2017.06.013

[6] Leung, K. T., Whidborne, J. F., Purdy, D., & Dunoyer, A. (2010). A review of ground vehicle dynamic state estimations utilizing GPS/INS. *Vehicle System Dynamics*, *49*(1–2), 29–58. https://doi.org/10.1080/00423110903406649

[7] Nam, K., Oh, S., Fujimoto, H., & Hori, Y. (2013). Estimation of sideslip and roll angles of electric vehicles using lateral tire force sensors through RLS and Kalman filter approaches. *IEEE Transactions on Industrial Electronics*, *60*(3), 988–1000. https://doi.org/10.1109/TIE.2012.2188874

[8] Baffet, G., Charara, A., & Lechner, D. (2009). Estimation of vehicle sideslip, tire force and wheel cornering stiffness. *Control Engineering Practice*, *17*(11), 1255–1264. https://doi.org/10.1016/j.conengprac.2009.05.005

[9] Doumiati, M., Victorino, A. C., Charara, A., & Lechner, D. (2011). Onboard real-time estimation of vehicle lateral tire-road forces and sideslip angle. *IEEE-ASME Transactions on Mechatronics*, *16*(4), 601–614. https://doi.org/10.1109/TMECH.2010.2048118

[10] Nam, K., Fujimoto, H., & Hori, Y. (2012). Lateral stability control of in-wheel-motor-driven electric vehicles based on sideslip angle estimation using lateral tire force sensors. *IEEE Transactions on Vehicular Technology*, *61*(5), 1972–1985. https://doi.org/10.1109/TVT.2012.2191627

[11] Li, L., Jia, G., Ran, X., Song, J., & Wu, K. (2014). A variable structure extended Kalman filter for vehicle sideslip angle estimation on a low friction road. *Vehicle System Dynamics*, *52*(2), 280–308. https://doi.org/10.1080/00423114.2013.877148

[12] Tsunashima, H., Murakami, M., & Miyataa, J. (2006). Vehicle and road state estimation using interacting multiple model approach. *Vehicle System Dynamics*, *44*, 750–758. https://doi.org/10.1080/00423110600885772

[13] Zhang, F., Wang, Y., Hu, J., Yin, G., Chen, S., Zhang, H., & Zhou, D. (2021). A Novel Comprehensive Scheme for Vehicle State Estimation Using Dual Extended H-Infinity Kalman Filter. *Electronics*, *10*(1526). https://doi.org/10.3390/electronics10131526

[14] Yang, F., Zheng, L., & Wang, J. (2019). Double layer unscented Kalman filter. *Acta Automatica Sinica*, *45*(7), 1386–1391. https://doi.org/10.16383/j.aas.c180349 (in Chinese)

[15] Wang, Z., Qin, Y., Gu, L., & Dong, M. (2017). Vehicle system state estimation based on adaptive unscented Kalman filtering combining with road classification. *IEEE Access*, *5*, 27786–27799. https://doi.org/10.1109/ACCESS.2017.2771204

[16] Mishra, A. K., Shimjith, S. R., & Tiwari, A. P. (2019). Adaptive unscented Kalman filtering for reactivity estimation in nuclear power plants. *IEEE Transactions on Nuclear Science*, *66*(12), 2388–2397. https://doi.org/10.1109/TNS.2019.2953196

[17] Hashemi, E., Kasaiezadeh, A., Khosravani, S., Khajepour, A., Moshchuk, N., & Chen, S.-K. (2016). Estimation of longitudinal speed robust to road conditions for ground vehicles. *Vehicle System Dynamics*, *54*(8), 1120–1146. https://doi.org/10.1080/00423114.2016.1178391

[18] Heidfeld, H., & Schünemann, M. (2021). Optimization-based tuning of a hybrid UKF state estimator with tire model adaption for an all-wheel-drive electric vehicle. *Energies*, *14*(5), 1396. https://doi.org/10.3390/en14051396

[19] Chen, J., Song, J., Li, L., Jia, G., Ran, X., & Yang, C. (2016). UKF-based adaptive variable structure observer for vehicle sideslip with dynamic correction. *IET Control Theory & Applications*, *10*, 1641–1652. https://doi.org/10.1049/iet-cta.2015.1030

[20] Chen, L., Bian, M., Luo, Y., & Li, K. (2016). Real-time identification of the tyre-road friction coefficient using an unscented Kalman filter and mean-square-error-weighted fusion. *Proceedings of the Institution of Mechanical Engineers, Part D: Journal of Automobile Engineering*, *230*, 788–802. https://doi.org/10.1177/0954407015595725

[21] Jin, X., & Yin, G. (2015). Estimation of lateral tire-road forces and sideslip angle for electric vehicles using interacting multiple model filter approach. *Journal of the Franklin Institute*, *352*, 686–707. https://doi.org/10.1016/j.jfranklin.2014.12.002

[22] Xin, X., Chen, J., & Zou, J. (2014). Vehicle state estimation using cubature Kalman filter. *IEEE 17th International Conference on Computational Science and Engineering*, 44–48. https://doi.org/10.1109/CSE.2014.42

[23] Matsushima, S., Tsujita, T., & Abiko, S. (2020, July). Distance control between an object and an end effector for contactless surface tracking works by a humanoid robot. *In 2020 IEEE/ASME International Conference on Advanced Intelligent Mechatronics (AIM)* (pp. 1724–1729). IEEE. https://doi.org/10.1109/AIM43001.2020.9159007

[24] Zhang, Z., Yin, G., & Wu, Z. (2022). Joint Estimation of Mass and Center of Gravity Position for Distributed Drive Electric Vehicles Using Dual Robust Embedded Cubature Kalman Filter. *Sensors*, *22*(21), 10018. https://doi.org/10.3390/s222410018

[25] Wang, Y., Geng, K., Xu, L., Ren, Y., Dong, H., & Yin, G. (2020). Estimation of sideslip angle and tire cornering stiffness using fuzzy adaptive robust cubature Kalman filter. *IEEE Transactions on Systems, Man, and Cybernetics: Systems, 52*(3), 1451–1462. https://doi.org/10.1109/TSMC.2020.3020562

[26] Yaming, L., Rongyun, Z., Peicheng, S., Linfeng, Z., Yongle, F., & Yufeng, D. (2022). Distributed Electric Vehicle State Parameter Estimation Based on the ASO-SRGHCKF Algorithm. *IEEE Sensors Journal*, *22*(18), 18780–18792. https://doi.org/10.1109/JSEN.2022.3199488

[27] Xiong, H., Liu, J., Zhang, R., Zhu, X., & Liu, H. (2019). An accurate vehicle and road condition estimation algorithm for vehicle networking applications. *IEEE Access*, *7*, 17705–17715. https://doi.org/10.1109/ACCESS.2019.2895072

[28] Hou, S., Xu, W., & Liu, G. (2019). Design of an interacting multiple model-cubature Kalman filter approach for vehicle sideslip angle and tire forces estimation. *Mathematical Problems in Engineering*. https://doi.org/10.1155/2019/6087450

[29] Schramm, D., Hiller, M., & Bardini, R. (2018). Single Track Models. In: Vehicle Dynamics. Springer, Berlin, Heidelberg. https://doi.org/10.1007/978-3-662-54483-9_10

[30] Cheng, S., Li, L., & Chen, J. (2017). Fusion algorithm design based on adaptive SCKF and integral correction for side-slip angle observation. *IEEE Transactions on Industrial Electronics*, *65*(7), 5754–5763. https://doi.org/10.1109/TIE.2017.2774771

[31] Shen C., Zhang Y., Guo X., Chen X., Cao H., Tang, J. Li, & Liu J. (2021). Seamless GPS/Inertial Navigation System Based on Self-Learning Square-Root Cubature Kalman Filter. *IEEE Transactions on Industrial Electronics*, *68*(1), 499–508, https://doi.org/10.1109/TIE.2020.2967671

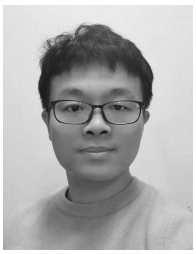

Yan Wang received the Ph.D. degree in mechanical engineering from Southeast University, Nanjing, China, in 2022. He was a research fellow with Nanyang Technological University. He is currently a research associate with the Hong Kong Polytechnical University. His current research interests include vehicle system dynamics and automotive active safety control. He has contributed to over 30 papers and obtained 15 patents. He is a Youth Editorial Board Member of the Chinese *Journal of Mechanical Engineering* and the *Journal of China.* He was also the recipient of the Outstanding Paper Award of *China Mechanical Engineering* in 2019, the Outstanding Reviewer Award of the *Chinese Journal of Mechanical* Engineering in 2022, the Excellent Doctoral Dissertation Award of Jiangsu Province in 2023, the Outstanding Doctoral Thesis Award of Southeast University in 2023.

Xianfang Wang (Senior Member of the China Computer Federation – CCF), graduated from Jiangnan University in 2009 with a Ph.D. in Control Theory and Control Engineering. From October 2014 to October 2015, she was a state-sponsored visiting scholar at the University of Missouri, Columbia, in the United States. From July 2023 to January 2024, she was a state-sponsored senior research scholar at Nanyang Technological University in Singapore. She is currently a professor at the School of Computer Science and Technology of Henan Institute of Technology. Her research interests include artificial intelligence, machine learning and their applications. She has been the principal investigator for 2 National Natural Science Foundation projects and more than 7 provincial-level projects and has published over 60 academic papers.

Xuan Sun received the M.Sc. degree in Safety Science and Engineering from the Beijing Jiaotong University, Beijing, China. She is currently pursuing the Ph.D. degree in Safety Science and Engineering from the School of Traffic and Transportation, Beijing Jiaotong University, Beijing, China. Her current research interests include spatiotemporal data mining, trajectory prediction, and safety state estimation based on interpretative machine learning.

Zhijuan Jia received the B.Sc. degree in Computer Applied Technology from Information Engineering University, Zhengzhou, China, in 1993, and the M.Sc. degree in Educational Technology from Beijing Normal University, Beijing, China, in 2006. Since 1993, she has worked at Zhengzhou Normal University, where she is currently a professor. She was a Visiting Scholar with the University of Wollongong, Australia, in 2017. She is an awardee of the National Science Fund of China and an academic leader of the Henan Science and Technology Department. She has published more than 30 papers and 2 monographs. Her research interests include information security and trusted computing.

Metrol. Meas. Syst., Vol. 31 (2024), No. 2, pp. 383–399
DOI: 10.24425/mms.2024.149705

Cui Dong is currently pursuing a Ph.D. degree from Tianjin University of Mechanical Engineering. His current research interests include vehicle state estimation and automotive active safety control. He has contributed to 5 papers and obtained 5 patents. He also won the first prize of the 2023 China Intelligent Transportation Association Science and Technology Progress Award and the second prize of the 2022 Tianjin Science and Technology Progress Award.

Zhiguo Zhang is currently pursuing his Ph.D. degree from the Department of Vehicle Engineering of Southeast University, Nanjing, China. His current research interests include vehicle state estimation and automotive active safety control. He has contributed to 5 papers and obtained 7 patents. He was the recipient of the First Prize of the Innovation and Development Award of the China Association of Productivity Promotion Centers in 2022 and 2023, Second Prize for Scientific and Technological Advancement in Tianjin Municipality in 2022.